A Modeling Study of Coastal-Trapped Wave Propagation in the Gulf of California. Part II: Response to Idealized Forcing

J. A. MARTÍNEZ* AND J. S. ALLEN

College of Oceanic and Atmospheric Sciences, Oregon State University, Corvallis, Oregon

(Manuscript received 5 August 2002, in final form 25 November 2003)

ABSTRACT

The propagation of incident coastal-trapped waves in the Gulf of California is investigated using a hydrostatic primitive equation model. The behavior of idealized incident wave disturbances with different amplitudes and time scales is examined. The incident wave disturbances propagate northward up-gulf along the east side with no significant change. At the sill, which is 600 km north of the entrance, the wave splits and most of the energy is steered to the west side where it propagates southward down-gulf with decreased amplitude (50%). A small fraction (10%–20%) of the incident energy enters the north where it is dissipated. Sea level at the entrance of the gulf is well correlated with sea level everywhere inside the gulf. In contrast, correlations of depth-averaged velocity between Topolobampo (close to the entrance of the gulf) and locations around the gulf decrease along the propagation path of the wave. Most of the dissipation of wave energy in the gulf takes place through bottom friction in the vicinity of the sill. Incident waves with large, but realistic, sea level displacement magnitudes exhibit nonlinear properties. Phase speeds increase as the sea level displacements of the incident waves increase from −30 to +30 cm. Waves of sea level elevation steepen. On the east side, large-amplitude elevation waves produce a down-gulf current adjacent to the coast such that the up-gulf currents associated with the wave separate from the coast. The separation process seems to be connected with subsequent downslope propagation of energy. Energetic anticyclonic eddies with spatial scales of 50–80 km can be generated by long-time-scale or large-amplitude elevation waves.

1. Introduction

Free coastal-trapped waves (CTWs) generated by hurricanes along the Pacific coast of Mexico have been observed propagating northward and entering the Gulf of California (GOC; Christensen et al. 1983; Enfield and Allen 1983; Merrifield 1992). These waves typically have periods of 4–20 days and sea level amplitudes at the coast of 20–30 cm. Inside the gulf, the waves are modified, as they are not observed on the Pacific side of the Baja California peninsula. In this two-part study, the evolution of remotely forced CTWs in the Gulf of California is investigated using a hydrostatic primitive equation model. In Part I (Martínez and Allen 2004), the model is forced by an incident mode-1 CTW with time-dependent amplitude derived from sea level observations south of the gulf during the 80-day period from 5 July to 23 September 1984. In Part II (this article), we complement the simulation in Part I by analysis of a set of experiments in which we vary the amplitude and the time scale of idealized incident wave pulses with single-signed displacements in coastal sea level. We study the behavior of the wave propagation in the gulf as a function of incident wave amplitude and time scale. An outline of the paper is as follows: The model formulation and the numerical experiments are described in section 2. Basic characteristics of the propagation and nonlinear effects are discussed in sections 3 and 4, respectively. A summary is given in section 5.

2. Model

We use the Princeton Ocean Model (POM) for the hydrostatic primitive equations (Blumberg and Mellor 1987). The model domain and the model parameters are the same as in Part I. The y coordinate is aligned in the along-gulf direction and is oriented toward the northwest, generally along the Baja California peninsula (see Fig. 1 in Part I). The orthogonal x coordinate has an across-gulf orientation directed toward the northeast. The velocity components in the (x, y) direction are (u, v). The open boundary conditions and the wave forcing are applied as discussed in Part I.

Waves generated south of the Gulf of California have been observed propagating poleward along the coast (Christensen et al. 1983; Enfield and Allen 1983). The

* Current affiliation: Facultad de Ciencias Marinas, Universidad Autonoma de Baja California, Ensenada, Mexico.

Corresponding author address: Dr. John S. Allen, College of Oceanic and Atmospheric Sciences, Oregon State University, 104 Ocean Admin Bldg., Corvallis, OR 97331-5503.
E-mail: jallen@coas.oregonstate.edu

observed phase speed is consistent with a CTW mode 1. To simulate incident waves at the south boundary, we specify the normal along gulf velocity v and the density ρ,

$$v_{\text{bdry}} = R_v(x, z)\phi(t) \qquad \text{and} \qquad (2.1a)$$

$$\rho_{\text{bdry}} = R_\rho(x, z)\phi(t), \qquad (2.1b)$$

where $\phi(t)$ is the time variability and $R_v(x, z)$ and $R_\rho(x, z)$ are the appropriate mode-1 structures calculated using the linear CTW model of Brink and Chapman (1987). In Part I, the time variability $\phi(t)$ is obtained from observed sea level data at Acapulco south of the gulf. In this study we investigate the propagation of idealized incident waves. To do this, we choose the time variability to represent a single isolated pulse given by

$$\phi(t) = A \operatorname{sech}^2(\alpha - \omega t), \qquad (2.2)$$

where A is the amplitude, ω^{-1} is the time scale, and α is a constant chosen so that the wave amplitude at the southern boundary increases smoothly in time.

To study the propagation characteristics of CTWs in the Gulf of California we conduct several experiments. The experiments can be divided in two sets: 1) single pulses with realistic topography and coastline and 2) single pulses with idealized topography and coastline. The amplitudes of the simulated incident CTWs, in terms of the displacements of sea level at the coast at Topolobampo ($y = 470$ km), are ± 2, ± 16, ± 22, and ± 30 cm and include values that represent very small waves and larger values that are typical of the observed events. Note that we use the terminology wave amplitude for the *signed* sea level displacements in the incident waves. We consider both elevation waves, with positive sea level displacements and positive amplitudes, and depression waves, with negative sea level displacements and negative amplitudes. Specified time scales range from 2 to 16 days and are consistent with the time scales of observed events.

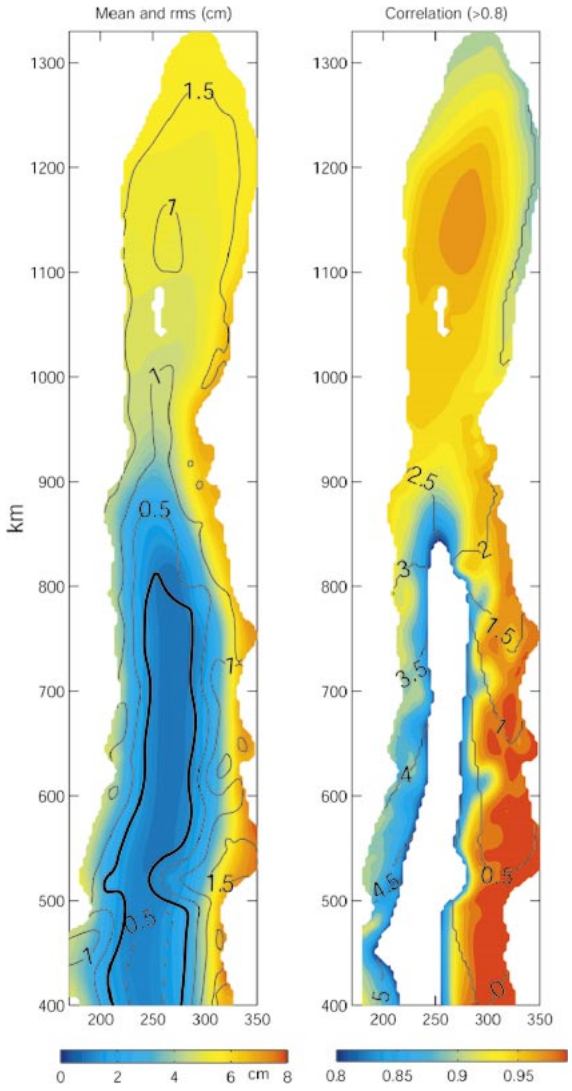

FIG. 1. (left) Temporal-mean (contour lines) and rms (color) fields of sea level and (right) the maximum correlations between sea level at Topolobampo ($y = 470$ km) and sea level at other locations in the gulf (color) and the corresponding lags (contour lines) in days for an incident elevation wave with amplitude 30 cm and time scale of 4 days. Only correlations >0.8 are plotted. The contour intervals for the lags are 0.5 days.

3. Propagation characteristics

a. Amplitude dependence

For a large-amplitude incident wave pulse of elevation (+30 cm) with a time scale of 4 days, we plot the temporal-mean and rms fields of sea level and the maximum lagged correlation of sea level at Topolobampo ($y = 470$ km) with other locations in the gulf in Fig. 1. The lag time in days for maximum correlation is also shown. The temporal-mean and rms sea level fields show that south of the sill, for $y < 900$ km, the surface elevation variations are confined near the coasts with larger magnitudes on the east side. The temporal-mean and rms values are also appreciable north of the sill where they show a tendency to spread across the full width of the gulf. For $y \leq 900$ km, the correlations are highest along the coast on the east side with somewhat smaller values along the coast on the west side. The time lags show that the wave propagates northward along the east side, turns near $y = 850$ km north of Santa Rosalia, and continues propagating southward along the west side. After a lag of 4.5 days, the wave is at $y = 500$ km on the western side of the gulf. A corresponding depression wave of the same magnitude and time scale takes approximately an extra day to propagate to the same location. That is, the depression wave propagates more slowly and spends more time in the gulf.

The maximum sea level correlations between Topolobampo ($y = 470$ km) and coastal stations inside the gulf at Guaymas ($y = 780$ km, east side), north gulf (y

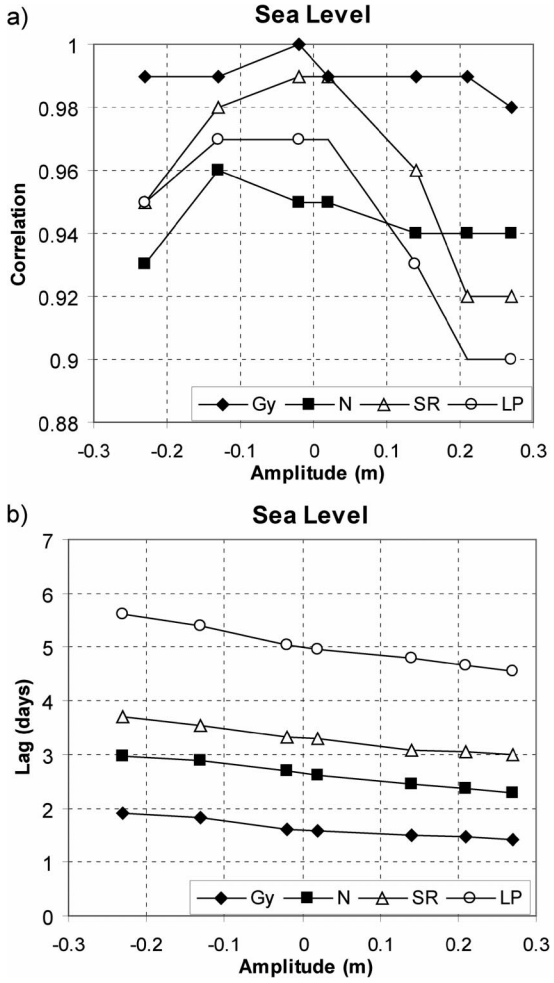

FIG. 2. (a) Maximum sea level correlations and (b) corresponding lags (days) between sea level at Topolobampo and sea level at Guaymas (Gy), north gulf (N), Santa Rosalia (SR), and La Paz (LP) as a function of the amplitude of the incident wave at Topolobampo. The incident wave has a time scale of 4 days. Sea level values were taken along the 100-m isobath.

$= 1330$ km), Santa Rosalia ($y = 800$ km, west side), and La Paz ($y = 470$ km, west side) (see Fig. 1 in Part I) as a function of the amplitude of an an incident CTW (ICTW) with a time scale of 4 days are summarized in Fig. 2. Note that the sea level amplitudes in Fig. 2 are measured on the 100-m isobath. The sea level signal is not strongly modified between Topolobampo and Guaymas, as indicated by the fact that the correlation is high and uniform for any ICTW amplitude. North of Guaymas at the sill, $y \approx 870$ km, the wave divides into two parts: 1) a small fraction of the energy continues to propagate northward along the eastern side and 2) the rest of the energy propagates southward along the western side (Fig. 1). The sea level correlations between Topolobampo and the north gulf station are the lowest of all stations for ICTWs with amplitudes less than +10 cm (Fig. 2). The correlations between Topolobampo and Santa Rosalia decrease relative to those between Topolobampo and Guaymas, with larger correlations for smaller-amplitude waves. A similar decrease is evident for correlations with La Paz. The corresponding sea level lags (Fig. 2) show an increasing propagation speed as the incident wave amplitude increases from −30 to +30 cm. Arrival at the north station leads that at Santa Rosalia by 18 h, and the lag difference between stations is independent of the amplitude. The lag at each station decreases linearly as the amplitude increases, showing that the phase speed increases approximately linearly with amplitude. After the ICTW passes Guaymas, the properties of the wave change. The dispersion diagram for the linear CTW mode 1 in the gulf in Part I shows much slower phase speeds in the northern gulf. The distance from Guaymas to the north gulf is about 480 km, and so the expected lag for a mode-1 CTW traveling from Guaymas to the north gulf should be much larger than the lag between Topolobampo and Guaymas (35–46 h for 312 km), given that the distance is greater and the mode-1 CTW phase speed is slower. The model phase speeds estimated from sea level, however, are on the order of 5.6–6.7 m s^{-1}, that is, 2 times the phase speed between Topolobampo and Guaymas (1.9–2.6 m s^{-1}).

The magnitudes of the complex correlation (Kundu 1976) of the depth-averaged velocity from water of depth 100 m at Topolobampo with depth-averaged velocities from similar water depths at other locations in the gulf as a function of the amplitude of the ICTW (Fig. 3) show some differences when compared with corresponding correlations of sea level. The velocity signal is strongly modified inside the gulf, resulting in lower correlations than found in the sea level signals. The magnitudes of the velocity complex correlations are typically larger for amplitudes near zero. The correlations at Santa Rosalia on the west coast are higher than those at Guaymas except for large-amplitude waves of elevation. At Santa Rosalia the magnitude of the complex correlation decreases rapidly for large amplitudes, suggesting that large-amplitude waves are strongly modified at the sill. Differences in behavior of the velocity fluctuations when compared with sea level can be seen from the lags (Fig. 3). In sea level, the lags show an anticlockwise propagation of the ICTW. For the velocity, the lags show that, after the signal passes Guaymas, it is subsequently detected at Santa Rosalia, and then La Paz. It arrives in the north gulf last. This indicates that the part of the ICTW that is observed in the velocity fluctuations in the north gulf has a phase speed reduced by 50%, to about 1.2 m s^{-1}, in agreement with the dispersion relation for a mode-1 CTW discussed in Part I. The lags at Guaymas, north gulf, and Santa Rosalia are smaller for small-magnitude waves. There is no consistent increase in phase speed with amplitude as seen in the sea level lags (Fig. 2). In fact, in the north gulf the lag increases significantly (roughly by 20 h) for waves with large sea level displacements, independent of sign. The relation between velocity lag

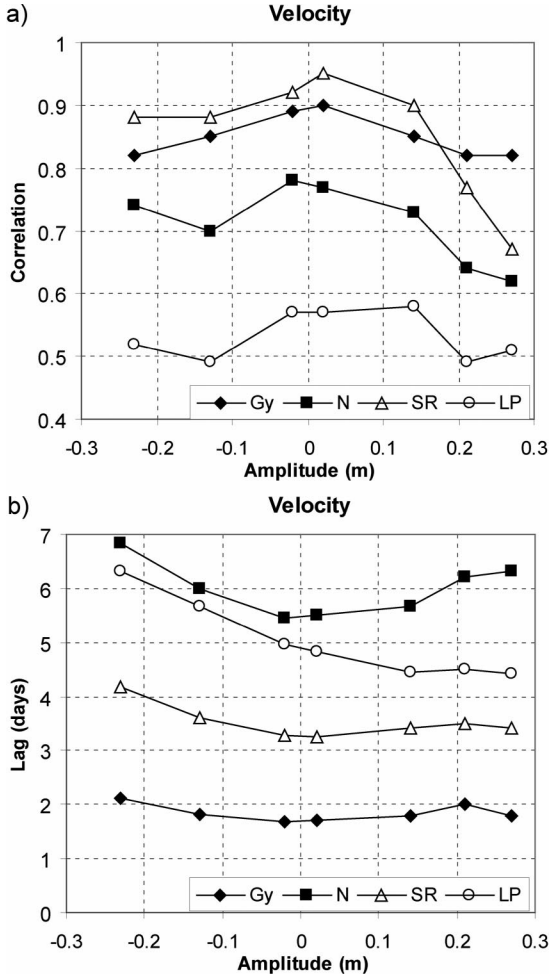

FIG. 3. Maximum correlations and lags as in Fig. 2 but for the depth-averaged velocities along the 100-m isobath. (a) The maximum magnitudes of a complex correlation coefficient. The correlation sign is reversed at stations N, SR, and LP. (b) The corresponding lags (days).

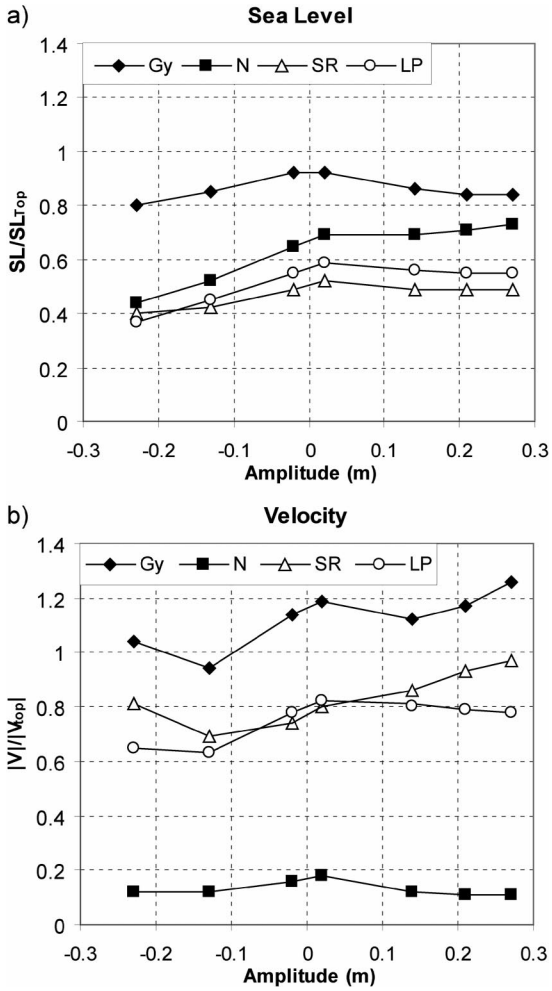

FIG. 4. Ratios of the maximum magnitudes at the same locations as in Fig. 2 to the maximum magnitudes at Topolobampo of (a) sea level ($\eta_t^{\max}/\eta_{\text{top}}^{\max}$) and (b) depth-averaged along-gulf velocity ($|V_t^{\max}|/|V_{\text{top}}^{\max}|$).

and amplitude at La Paz is similar to the one obtained for sea level (Fig. 2) except that for amplitudes larger than 12 cm the lag in velocity remains constant. In general, as for the sea level lag, velocity lag is larger for depression waves. Increasing amplitudes for elevation waves result in increasing lags in the north and nearly constant lags at the other locations.

The maximum magnitude of the sea level fluctuations decreases as the waves propagate along the gulf (Fig. 4a). At Guaymas the magnitude of the wave decreases by 10%–20% depending on the amplitude of the incident wave. At La Paz the magnitude has decreased by 40%–63%. Santa Rosalia sea level amplitude is about 3%–7% smaller than at La Paz. The relation between the maximum magnitude of the sea level fluctuations and the magnitude at Topolobampo is more strongly modified for depression waves (Fig. 4a). Depression wave magnitudes decrease 5%–30% more than those of the corresponding elevation waves. Waves of small absolute amplitude generally have the smallest decrease in magnitude except in the north gulf.

The maximum depth-averaged, along-gulf velocity magnitude (Fig. 4b) generally increases between Topolobampo and Guaymas for almost any amplitude. After the ICTW passes Guaymas, part of the wave continues north, but the velocity associated with this wave is relatively small, representing 10%–20% of the ICTW velocity at the gulf entrance. Santa Rosalia has a similar variation of velocity magnitude with ICTW amplitude as that found at Guaymas, but with a decrease in the values by 20%–40% with respect to Guaymas. The CTW leaving the gulf (close to La Paz) has a velocity magnitude that represents 60%–80% of the velocity magnitude of the ICTW at the entrance to the gulf, with higher values found for elevation waves.

The wave exiting the gulf at La Paz shows a sea level signal that is approximately 0.5 times the amplitude of

the incident wave at Topolobampo (Fig. 4), but the correlation does not decay significantly (Fig. 2). The decrease in maximum depth-averaged, along-gulf velocity (~20%) is not as strong as the one in sea level (~50%), but the signal has been strongly modified and is poorly correlated with the ICTW at Topolobampo (Fig. 3).

b. Time-scale dependence

To study the evolution of ICTWs inside the gulf as a function of the time scale of the incident wave, we consider ICTWs of moderate amplitude (±16 cm at Topolobampo) and we vary the time scale. We consider time scales of 2, 4, 8, and 16 days for both elevation and depression waves. The evolution of the ICTW inside the gulf as a function of time scales shows less sensitivity than found for the amplitude variations in section 3a. Sea level correlations with Topolobampo for these waves (not shown) are generally high. The lowest correlation (0.89) is between La Paz and Topolobampo for a depression ICTW with time scale of 2 days. Correlations for longer period waves tend to increase. The corresponding lag does not show any dependence on the time scale of the ICTW and the sea level signal propagates anticlockwise with the north leading Santa Rosalia by 17 h.

The velocity is more sensitive than sea level to the time scale of the ICTW. For elevation waves, the correlation decreases as the time scale increases (Fig. 5). Guaymas and Santa Rosalia have a similar behavior and are well correlated with the ICTW at Topolobampo. At La Paz the correlation drops abruptly by 30%–50% compared to the correlation at Santa Rosalia. The decreasing correlation for longer waves seems to be related to the generation of eddies and the separation of coastal currents (section 4). The lag for elevation waves, with time scales 4 days and less (Fig. 5), has a variation similar to that shown in Fig. 3 with the signal arriving first at Guaymas, second at Santa Rosalia, next at La Paz, and last in the north (Fig. 5). For a time scale of 8 days, the maximum correlation lag is the same for Santa Rosalia and La Paz. Waves with a time scale of 16 days are detected first at La Paz, then at Santa Rosalia. In general, for elevation waves the maximum relative sea level and velocity fluctuations increase at almost all stations as the time scale increases and the lag increases as the time scale increases (not shown). The correlation for depression waves does not change substantially as a function of the time scale.

c. Behavior in the northern gulf

Interesting behavior is found when the CTW arrives at the sill (y = 870 km). The Guaymas basin, located south of the sill, is 2000 m deep (Fig. 1 in Part I). In contrast, north of the sill the gulf is significantly shallower (~200 m). Shallow depth contours along the east shelf extend to the north gulf. For depths greater than 500 m, however, the contours separate from the east coast and turn south along the Baja California side. We illustrate the behavior in the north gulf by examining the evolution of a large-amplitude (~30 cm) elevation ICTW of time scale 4 days in Figs. 6, 7, and 8. The incident CTW in this case splits into two waves. A small fraction of the energy enters the north gulf and the rest of the wave turns back and propagates southward along the west coast of the gulf. Analysis of sea level and velocity fluctuations in the north gulf suggest the excitation of two wavelike motions with different properties: a fast-propagating sea level signal with an average phase speed of about 6 m s^{-1} that arrives at the north gulf station about 24 h after the wave passes Guaymas (Fig. 2) and a slow velocity signal consistent with a CTW with average phase speed of 1.2 m s^{-1} that arrives at the north station about 4.5 days after the wave passes Guaymas (Fig. 3).

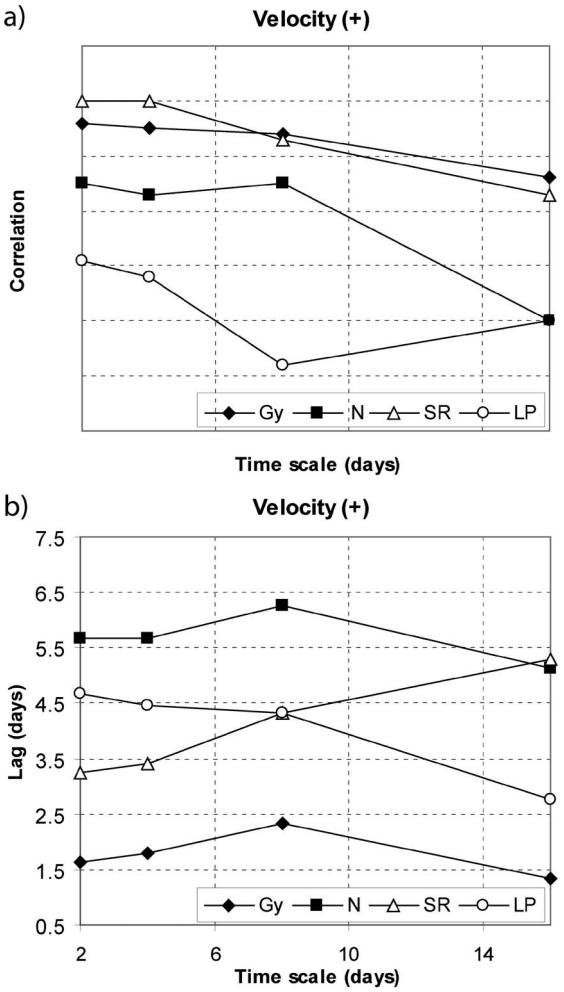

FIG. 5. Maximum correlations and lags for depth-averaged velocities as in Fig. 3 for incident elevation waves with an amplitude of +16 cm as a function of the incident wave time scale.

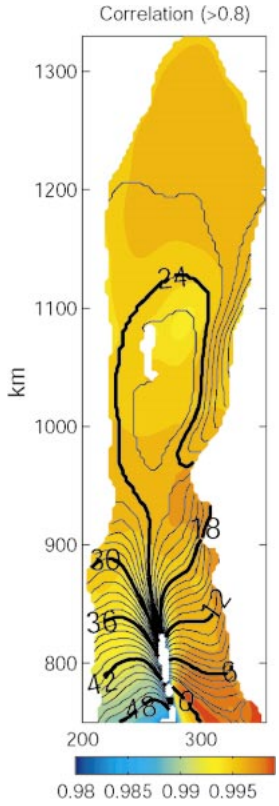

FIG. 6. Maximum correlations between sea level at a location on the coast along the east side at $y = 750$ km and sea level at other locations in the north gulf (color) and the corresponding lag (contour lines) in hours for an elevation ICTW with amplitude 30 cm and time scale of 4 days.

The maximum correlation and corresponding lag between sea level at a location on the coast along the east side at $y = 750$ km and sea level at other locations in the north gulf is shown in Fig. 6. On the east side south of $y = 850$ km, lines of constant lag extend perpendicular to the coast with increasing lag toward the north. Off the coast at $y = 850$ km, the phase of the wave shows westward propagation while the phase on the shelf continues to follow the coast. The result is a CTW that is steered, from northward propagation along the east coast to southward propagation along the west coast, about a pivotal point ($y = 850$ km) in the center of the gulf. North of Tiburon Island ($y = 960$ km) the correlations are high. The phases show some continued CTW-like propagation along the coast on the east side south of $y = 1100$ km. The slow-propagating signal on the east side vanishes in the north.

A comparison of the propagation of sea level and velocity signals in the north (Fig. 7) reveals features consistent with those discussed in connection with the analysis of correlation coefficients (Figs. 2 and 3). The time-dependent behavior of the velocity field in the north seems to reflect a different type of wave behavior than that shown by the evolution of sea level (Fig. 7). At day 9 high sea level extends to the north gulf, while the velocity signal is just passing Tiburon Island ($y = 960$ km on the east side). By day 10 sea level is already decreasing in the north, while a CTW continues to propagate north along the coast on the east side close to $y = 1060$ km. Finally, on day 11 sea level returns to equilibrium and the velocity signal is weak. Evolution of the along-gulf velocity component during the same days (Fig. 8) shows a velocity signal north of the sill propagating northward at a slow speed that is not observed for sea level (Fig. 7). The velocity signal resembles a CTW strongly modified by topography, with an offshore scale larger than that of the incident wave south of $y = 700$ km (Fig. 8). The velocity signal eventually decays and a signal propagating southward along the west side of the north gulf is not evident.

Bottom friction in the shallow northern gulf has been the most popular mechanism used to explain the observed weakening of ICTWs (Merrifield 1992; Ramp et al. 1997). In Part I, it is found that just a small fraction of the ICTW energy enters the north gulf and that dissipation in the north is not enough to explain the weakened signals along the west side of the gulf. The time-integrated kinetic energy balance of the depth-averaged velocities integrated over depth and in the across gulf direction (Fig. 9) shows that the flux of energy into the gulf is balanced mainly by dissipation due to bottom friction. Total dissipation due to bottom friction is very uniform from the south gulf to the sill. Both energy flux and bottom dissipation are small north of the sill, showing that a very small fraction of the ICTW enters the north gulf. At the sill kinetic energy flux and bottom dissipation are relatively large, and bottom dissipation values are the highest along the gulf. The kinetic energy density balance (i.e., the integrated kinetic energy balance divided by the volume of the across-gulf section; Fig. 9) shows that at the sill, as the gulf narrows and the depth decreases from 2000 to 400 m, the energy flux density increases. This intensified flux of energy is balanced by bottom dissipation. No significant increase in either the total dissipation or the dissipation per unit volume is observed in the north gulf for ICTWs with different amplitudes and time scales.

4. Nonlinear effects

Storm-generated disturbances along the coast of Mexico have been observed propagating northward over long distances (Enfield and Allen 1983). The signals appear as isolated waves of elevation with amplitudes of 20 cm or more. In contrast, depression waves generated during winter in the neighborhood of the Gulf of Tehuantepec on the south Pacific coast of Mexico near 16°N do not seem to propagate northward as nondispersive signals. The relative longevity of elevation waves suggests a wave evolution governed by Korteweg–de Vries (KdV) type dynamics with weak nonlinear effects balanced by dispersion. Theoretical models

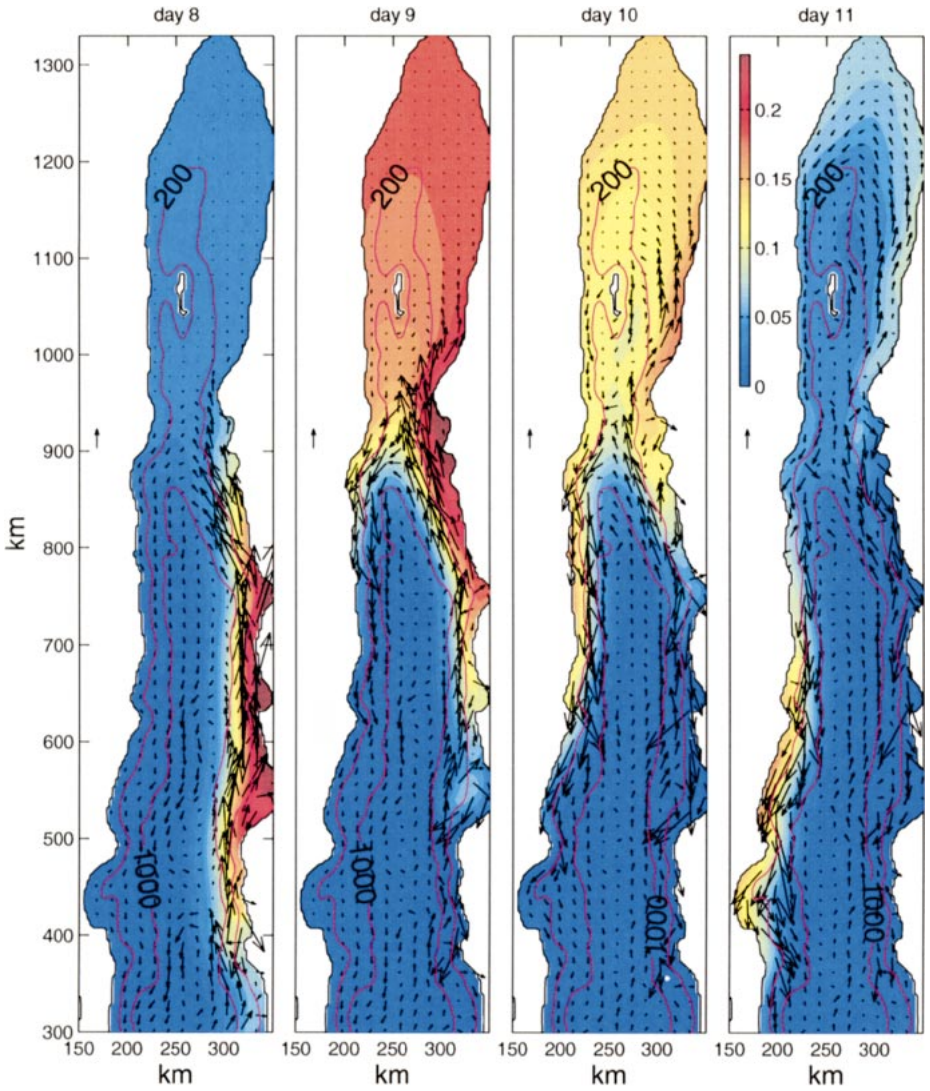

FIG. 7. Depth-averaged velocity vectors and sea level (color) on days 8–11 for an elevation ICTW with amplitude 30 cm and time scale of 4 days. The velocity vector scale to the left in each panel corresponds to 20 cm s^{-1}.

for weakly nonlinear barotropic shelf waves have been formulated by Smith (1972) and Grimshaw (1977). These models show that nonlinear solitary waves may exist for across-shelf mode 1 as waves of sea level elevation, but not as waves of depression. A formulation for nonlinear stratified CTWs is included in Mitsudera and Grimshaw (1990), although the emphasis there is on resonant forcing of mode 2 by topographic features. Nonlinear effects could be in part responsible for some inconsistencies between observed seasonal changes in propagation speed for free waves and the phase speed predicted by linear theory (Enfield and Allen 1983).

a. Wave steepening

In these numerical experiments we find a dependence of the phase speed on the amplitude of the incident wave as discussed in section 3a. The phase speed of the sea level signal increases linearly with the amplitude of the wave (Fig. 2). The phase speed of the velocity signal also increases with amplitude for depression waves, but for elevation waves the phase speed does not appear to vary significantly (Fig. 3). The dependence of CTW phase speed on incident wave amplitude is clearly seen in comparative time series of sea level (Fig. 10). As the signals propagate, the crests of the waves of different initial amplitudes separate in time, such that on the east side, at $y = 744$ km, the crest of the largest elevation wave leads the crest of the largest depression wave by 2 days. Large elevation waves steepen at the front, while the depression waves steepen of the tail. The sea level displacements of depression waves decrease in magnitude 50% or more while they propagate along the east side (Fig. 10), while elevation waves do not change

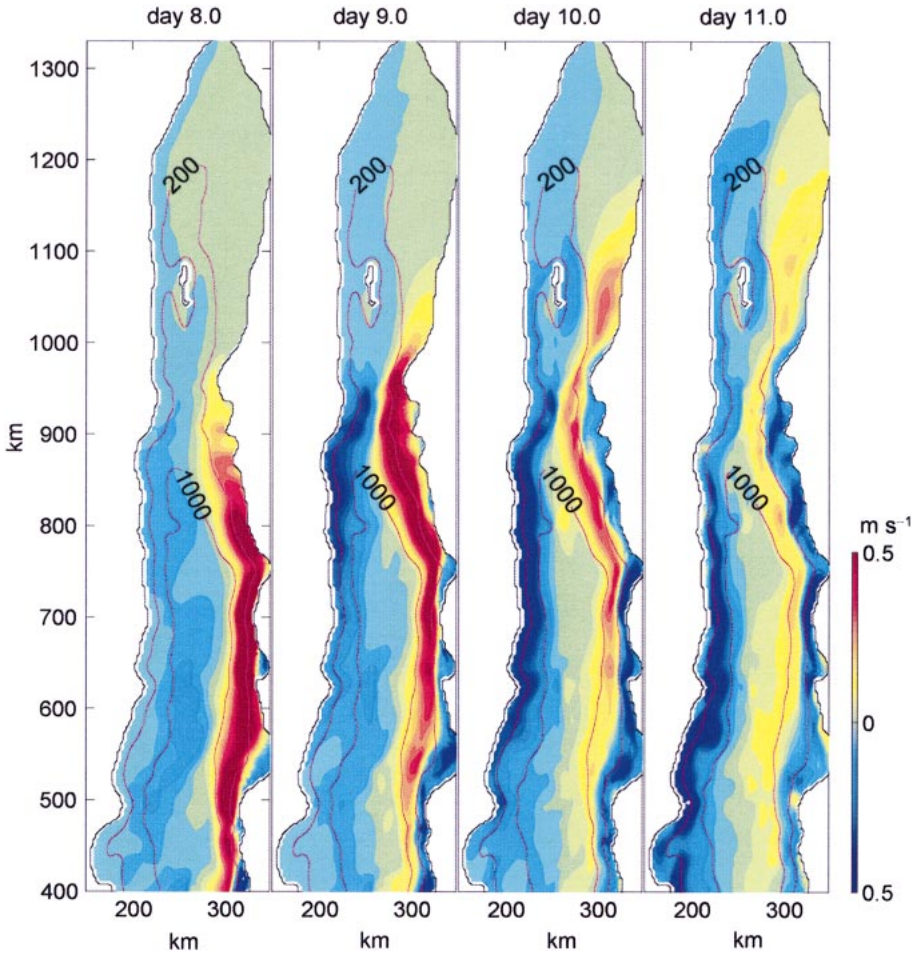

FIG. 8. Fields of the along-gulf depth-averaged velocity for the same experiment and days as in Fig. 7.

amplitude significantly there. On the west side elevation waves decrease in amplitude by 30%, while there is less noticeable amplitude change in depression waves.

As found in section 3a, the alongshore velocity shows some behavior not seen in the sea level signals. The dependence of the phase speed on the amplitude found from sea level is also evident in the alongshore component of the depth-averaged velocity (V) (Fig. 11). As in the sea level signals, elevation waves, with positive alongshore velocity ($V > 0$) on the east side and negative ($V < 0$) on the west side, preserve the initial shape and amplitude of the incident wave better than depression waves. Dispersive effects behind the main wave are evident in the velocity signal. Waves with a given sign generate a secondary trailing wave of opposite sign. The sea level amplitude of the secondary wave is small in comparison with the amplitude of the main wave (Fig. 10), but the magnitude of depth-averaged alongshore velocity (V) of the secondary wave is comparable to the velocity associated with the main wave (Fig. 11) in the gulf on the east side. As the wave propagates northward, some steepening in velocity occurs at the front (tail) of elevation (depression) waves.

It is interesting to compare the time series of sea level and along-gulf velocity of the CTWs in Figs. 10 and 11 with time series for the depths of isopycnals shown in Fig. 12. Elevation waves produce a sinking of isopycnals, while depression waves produce isopycnal rising. The vertical displacements are larger below 50 m for both elevation and depression ICTWs. Note that the gradients that develop in the isopycnal depths (Fig. 12) are considerably stronger than those in sea level (Fig. 10). Depression waves steepen at the tail. Behind the tail higher-frequency disturbances seem to be generated, but the leading part of the wave shape is not highly distorted. The elevation wave also generates high-frequency disturbances as the crest passes $y = 384$ km. It appears that, as the elevation wave propagates to $y = 564$ km, the high-frequency disturbances weaken and the isopycnal displacements vary more smoothly. Subsequently, at $y = 744$ km the wave appears to be steepening again and generating additional high-frequency fluctuations.

The relative importance of the nonlinear terms in the alongshore momentum balance is highly dependent on the amplitude of the incident wave. We find for waves

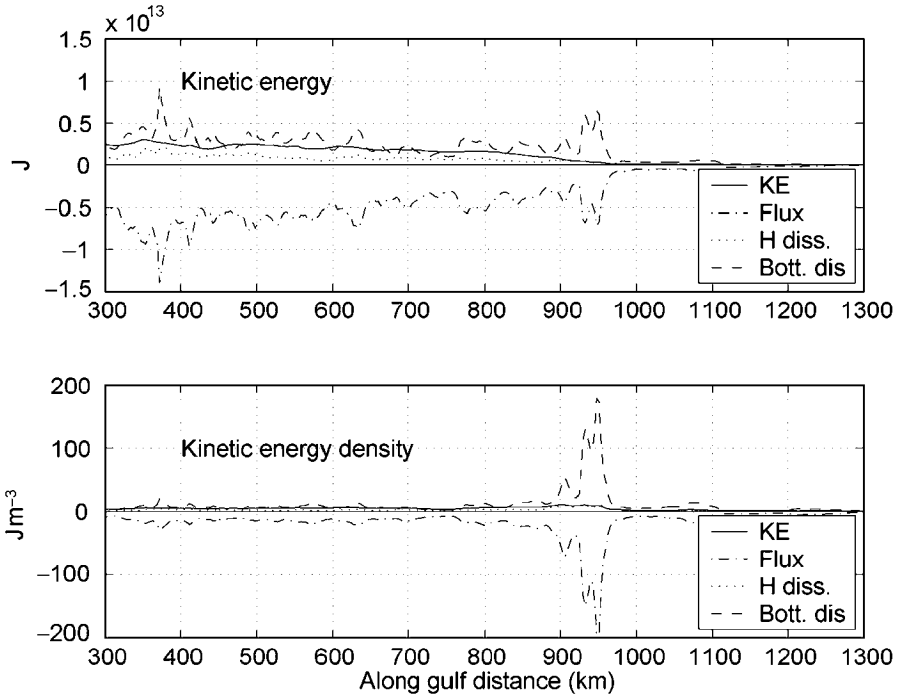

FIG. 9. Time-integrated kinetic energy balance of the depth-averaged velocities, integrated in the across-gulf direction, e.g., $\Delta y \int (\varphi)\, dx\, dt$, where φ represents the terms (time derivative, flux, dissipation due to horizontal friction, dissipation due to bottom friction) in the equation for the kinetic energy of the depth-averaged velocity. In the bottom panel, the terms are divided by the volume to give the volume average kinetic energy balance, $(\Delta y \int dx\, dz)^{-1} \Delta \int (\varphi)\, dx\, dt$). Note the flux term includes all terms not associated with the time derivative, horizontal diffusion, or bottom friction.

with large-magnitude sea level displacements that the nonlinear advection terms can be appreciable and, for elevation waves, can be one of the dominant terms. Time series of terms in the depth-averaged along-gulf momentum balance at five locations on the 200-m isobath along the east side of the gulf for elevation and depression ICTWs of amplitude ±30 cm are shown in Fig. 13. Before the ICTW enters the gulf (y = 180 km), nonlinear terms are nonnegligible but are relatively small in comparison with the acceleration, the Coriolis force, and the pressure gradient terms for both elevation and depression waves. Interestingly, at y = 180 km the nonlinear terms have the same sign in both the elevation and the depression wave, while the signs of the other terms are reversed. After the elevation ICTW enters the gulf (y = 384 km), nonlinear advection becomes one of the dominant terms and it remains large for all y locations to y = 924 km. In contrast, for the depression ICTW the nonlinear terms remain at about the same small relative magnitude in the gulf as at y = 180 km. Significant nonlinear effects are found for elevation waves with sea level amplitudes of 20 cm or larger. For medium-amplitude ICTWs (~15 cm), nonlinear advective effects occasionally make a significant contribution to the balance but are not as large as the other terms.

The model results clearly show that nonlinear effects can alter the propagation characteristics of CTWs with amplitudes of the same magnitude as those observed. These characteristics include wave steepening and the notable differences in behavior of elevation and of depression waves. Additional theoretical analysis of nonlinear aspects of CTW propagation with realistic stratification and topography to better understand the dynamical processes involved would be of interest.

b. Current separation

The contribution of nonlinear terms to the total momentum balance is dependent on the amplitude of the ICTW and on the position. Topography and coastline modify the incident wave propagation, leading to complex circulation patterns if the amplitude of the wave is large enough to develop nonlinear behavior. The evolution of the alongshore velocity component for an elevation ICTW of 30-cm amplitude and 4-day period (Fig. 8) shows the time-dependent development of these circulation patterns. An elevation ICTW is accompanied by up-gulf northward velocity fluctuations clearly visible along the east side of the gulf (Figs. 7 and 8). After approximately the first half of the wave has passed y = 750 km on day 9, however, a southward countercurrent develops next to the coast. The down-gulf southward current then propagates with the ICTW in such a way that, on day 10 at the tail of the wave, the up-gulf current

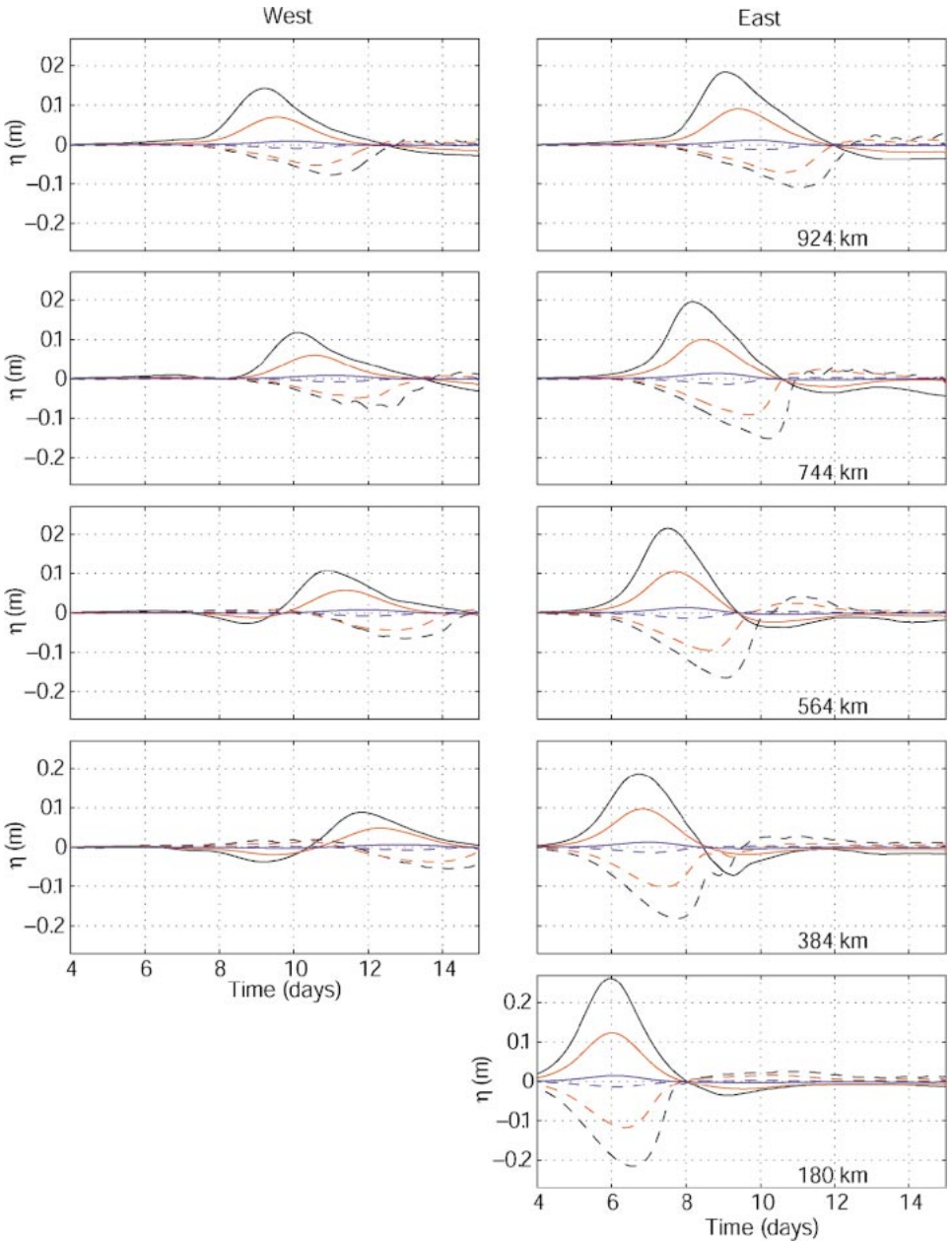

FIG. 10. Time series of sea level along the 100-m isobath at different locations along the gulf (right) from the east and (left) from the west side. Each curve represents a different experiment (total 6) where the amplitude of the incident wave is varied. The time scale for all experiments is 4 days. The initial amplitudes are ±30 cm (black), ±16 cm (red), and ±2 cm (blue), and waves of depression are dashed.

associated with the ICTW is separated from the coast by a down-gulf current that resembles the offshore structure of a mode-2 depression wave. On days 10 and 11 the width of the down-gulf current increases near the sill in the region between $y = 800$ and 950 km. By day 11 the secondary wave on the east side has separated from the primary wave that is now propagating southward along the west side. The secondary wave on the east side seems to continue propagating northward into the north gulf with reduced phase speed and decreased up-gulf velocity.

The temporal-mean along-gulf surface velocities for elevation waves with amplitudes 2 and 30 cm and time scales of 4 days are shown in Fig. 14. The small-amplitude (2 cm) elevation wave produces a mean surface circulation with positive up-gulf currents along the east side and negative down-gulf currents along the west side. The currents along both sides are fairly uniform

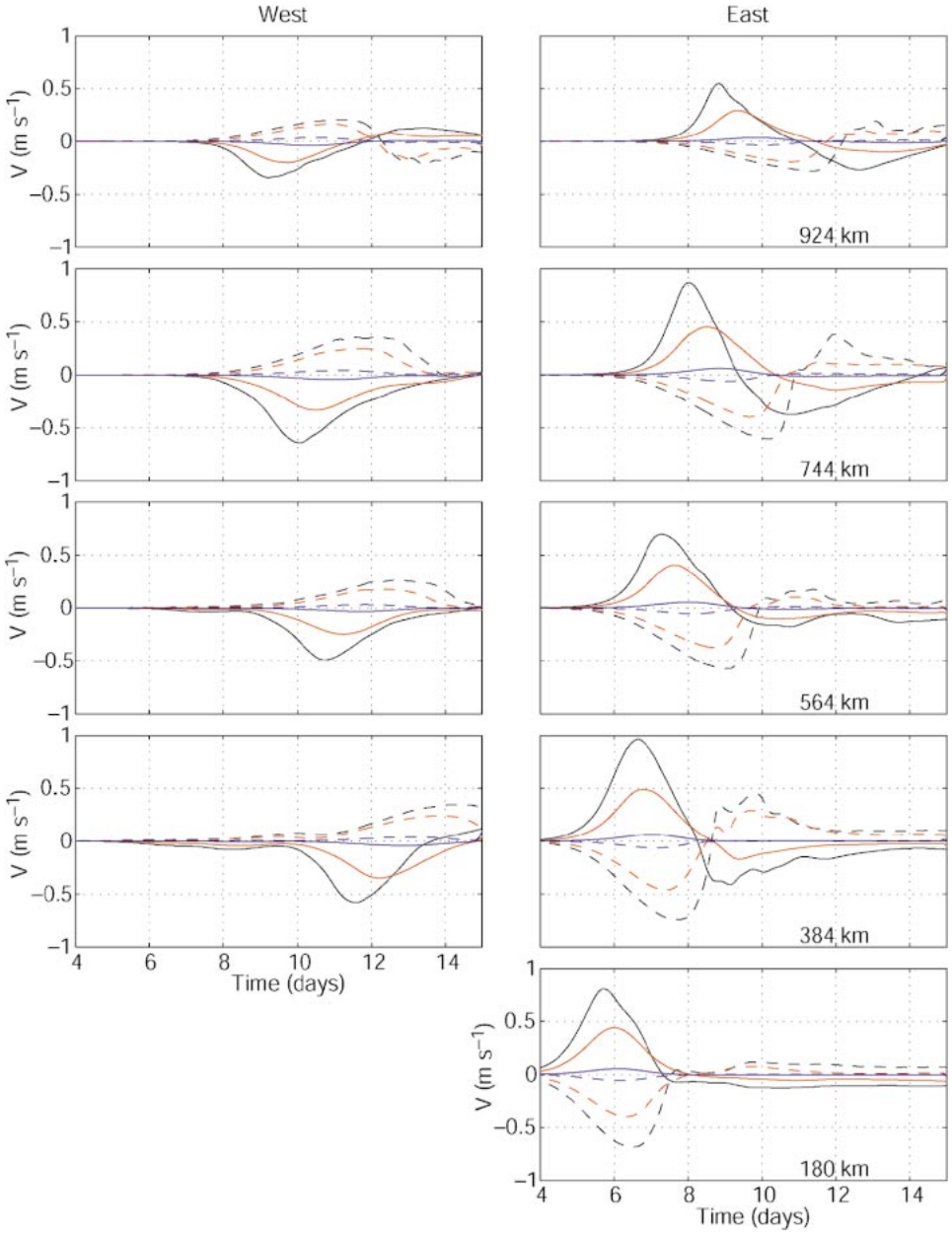

FIG. 11. As in Fig. 10 but for the depth-averaged velocity.

and contiguous to the coast. For the larger-amplitude (30 cm) elevation wave, the mean surface velocity along the east side shows an up-gulf current that has separated from the coast with a down-gulf countercurrent next to the coast. Along the west side the separation of the down-gulf current is weaker although still present to some extent. The separation of the basic current associated with the ICTW and the development of a countercurrent adjacent to the coast is found only for elevation waves with sea level amplitudes 16 cm or larger. For small elevation waves the temporal-mean alongshore velocity of the ICTW does not separate, even though after the wave passes there is a secondary wave with down-gulf currents next to the coast.

These results suggest that many of the observed ICTWs that propagate into the gulf have the potential to develop circulation patterns similar to those shown in Fig. 8. This is consistent with the fact that the formation of a countercurrent and the separation of the wave tail are also observed in Part I with realistic forcing. On the west side, where the alongshore velocity associated with an elevation ICTW is down-gulf, weak up-gulf currents adjacent to the coast are generated (Fig. 8), but separation similar to that found on the

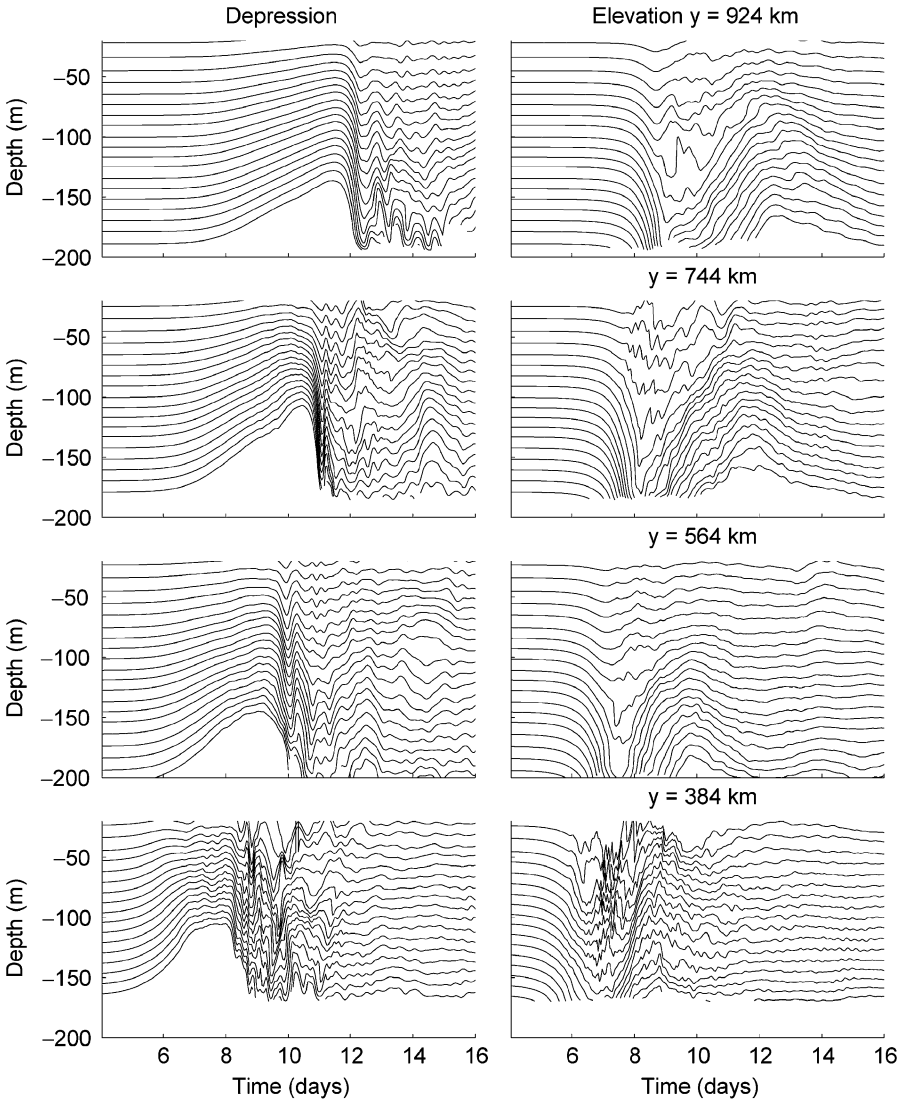

FIG. 12. Time series of isopycnal depths along the 200-m isobath on the east side. (right) A 30-cm elevation wave, and (left) a −30 cm depression wave at the same values of *y*. The time scale of the wave is 4 days. The isopycnals are chosen to have a uniform distribution of initial depth as shown for small time at $y = 924$ km.

east side is not observed even for large-amplitude waves.

In the south on the east side, the up-gulf current associated with the incident wave seems to propagate slowly offshore, for example, at $y = 570$ km in Fig. 8. The offshore propagation in the south gulf of the currents associated with the ICTW wave seems to be related to the downslope propagation observed in Part I. It is found there that after an elevation wave passes and separation begins to take place, the separated up-gulf velocity signal propagates downslope to the deepest part of the section. The changes in the vertical and across-gulf structure of the alongshore velocity as an elevation wave passes (Fig. 15) shows that process here. After the up-gulf current begins to separate on day 9, it begins to propagate downward along the bottom. By day 13 the vertical average of the along-gulf velocity is very weak (Fig. 8), but an up-gulf current is still found at the bottom of the section (Fig. 15) where it persists and gradually weakens. In Part I, downslope propagation that reaches the bottom is observed only along the east side of the gulf for incident elevation waves. In this study we find consistent results, as downslope propagation that reaches the bottom is not found for incident depression waves of any amplitude or time scale. Elevation waves with amplitudes larger than 5 cm in sea level and any time scale result in downslope propagation.

In an attempt to understand better the causes of the separation and of the development of the countercurrent

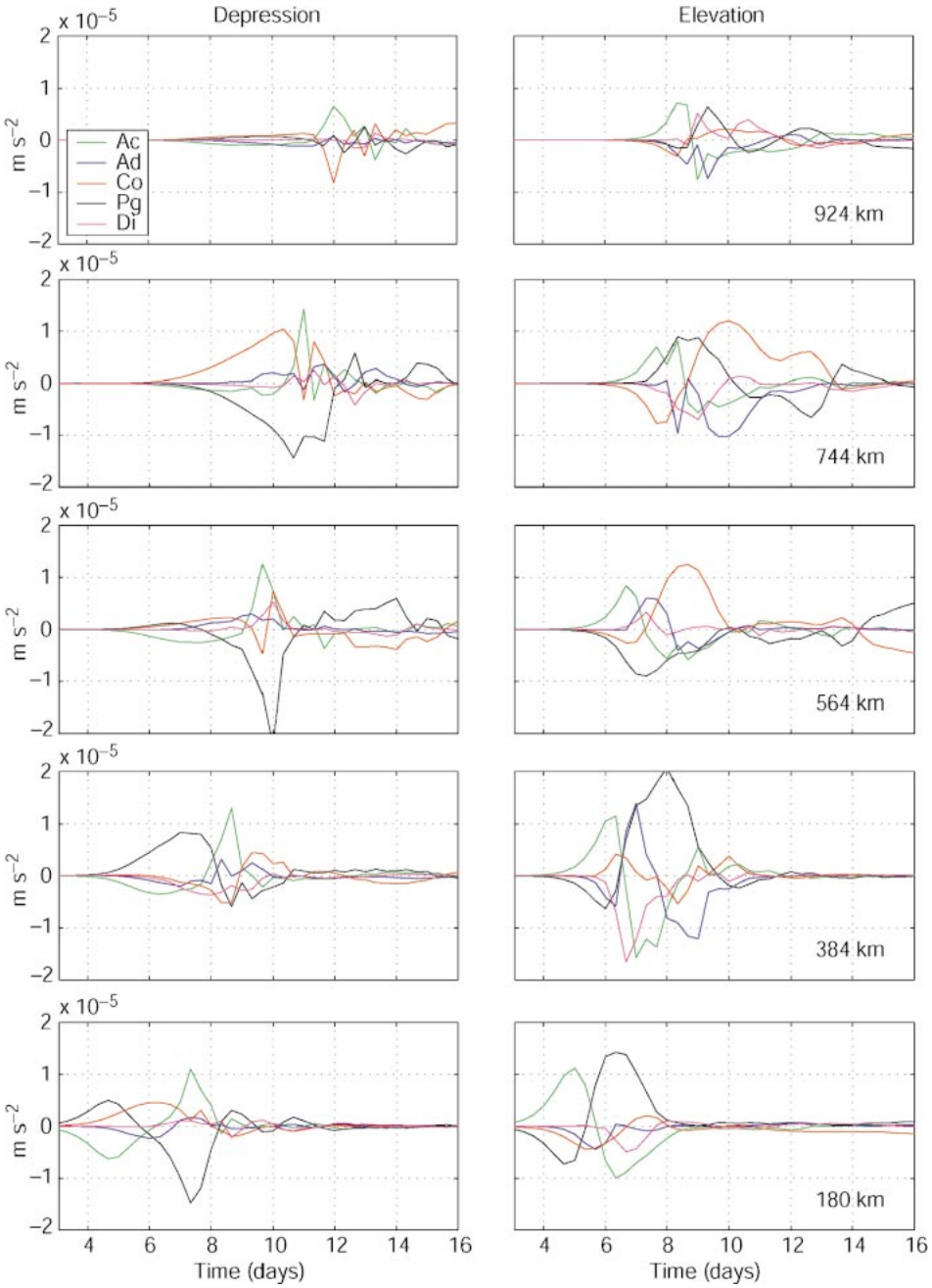

FIG. 13. Time series of terms in the depth-averaged along-gulf momentum equation at five locations on the 200-m isobath along the east side of the gulf. (right) A 30-cm elevation wave, and (left) a −30 cm depression wave at the same values of y. The bottom panels are from a location (y = 180 km) south of the entrance to the gulf, which is at y = 300 km. The sill begins at y = 828 km; Ac: acceleration, Ad: advection, Co: Coriolis, Pg: pressure gradient, and Di: diffusion terms.

we have run some additional numerical experiments. First, we utilize a rectangular channel with dimensions similar to the gulf and a constant depth of 1000 m forced by an incident first-mode baroclinic Kelvin wave. No countercurrent or separation is observed for incident elevation waves of any amplitude. A second experiment has a constant depth of 1000 m, similar to the first one, but includes the actual coastline of the gulf. In this case, a narrow countercurrent develops similar to the one shown in Fig. 8. As the wave passes, small anticyclonic eddies are generated in the inlets and bays and these propagate slowly westward. In two additional experiments, the average across-gulf depth of the gulf is used so that the depth is a function of the along-gulf coor-

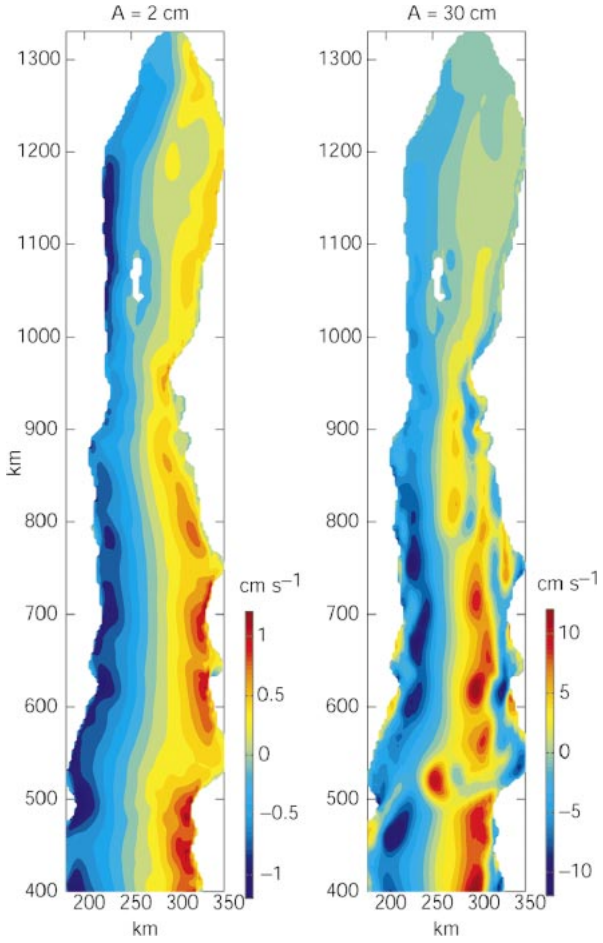

FIG. 14. Time-mean along-gulf surface velocity for (left) a small-amplitude elevation wave of 2 cm and (right) a large-amplitude elevation wave of 30 cm. The incident waves have a time scale of 4 days.

dinate only, both in a rectangular channel and in a channel with realistic coastline. In both cases, the wave is strongly modified by the topography. No countercurrent or separation is observed in the experiment in the rectangular channel. The inclusion of a realistic coastline produces a narrow countercurrent and some weak eddies. Overall, the experiments indicate that separation and the formation of countercurrents are nonlinear effects influenced by both the coastal shelf and slope topography and by irregularities in the coastline.

c. Eddy generation

One possible mechanism for energy dissipation of ICTWs in the Gulf of California is the generation of mesoscale eddies (Christensen et al. 1983). Mesoscale eddies have been frequently observed in the gulf (Badan-Dangon et al. 1985; Emilson and Alatorre 1997; Pegau et al. 2002; Figueroa et al. 2003), but to our knowledge, the only other modeling study that produces eddies in the south gulf is that by Martínez and Allen (2002, manuscript submitted to *J. Phys. Oceanogr.*) where the formation of eddies in the south gulf is found in wind-driven numerical experiments. In this study, we present some results that show eddy generation by ICTWs and we describe some of their main characteristics.

The formation of a countercurrent by an elevation ICTW is discussed in section 4b. The countercurrent flows southward down-gulf adjacent to the coast in such a way that for large-amplitude waves the up-gulf currents associated with the elevation ICTW separate from the coast. The development of the countercurrent and the separation of the wave tail are illustrated in Figs. 7 and 8. When the wave passes inlets along the east side, the up-gulf current of the ICTW induces anticyclonic circulation inside the bay for example, on day 9 at $y = 540$ m in Fig. 7. If the ICTW has a long time scale or large amplitude, anticyclonic eddies with length scales of 50–80 km are generated (Fig. 16). In addition, the circulation pattern produced by elevation waves along the east side, with an up-gulf current separated from the coast and a countercurrent adjacent to the coast (Fig. 8), provides strong horizontal shear conducive to the formation of anticyclonic eddies. The positions where the eddies are generated (Fig. 16) seem to be related to the locations of the largest variations in the coastline. The horizontal scale of the eddies is similar to the width of the shear zone adjacent to the coast and to the size of the coastline irregularities. Most of the eddies propagate westward at a very low speed ($\sim$3 cm s^{-1}) and are observed to last for at least 25 days after the wave passes with maximum velocities of 20 cm s^{-1} or more. In the vertical, the signature of the eddies typically extends to 200 m and in some cases reaches 500-m depth. Depression waves do not produce separation or a countercurrent, even though a few cyclonic eddies are generated mainly in the south gulf on the west side close to La Paz.

Long elevation waves (time scale of 8 days or greater) of moderate sea level amplitude ($\sim$16 cm) produce larger and stronger eddies than short waves (4 days time scale) with large amplitudes ($\sim$30 cm). The generation of eddies is also observed in the additional experiments described in section 4b, where we utilize a flat bottom in a rectangular channel or with a realistic coastline. In the rectangular channel, the formation of eddies is observed only on the west side near the tip of the Baja California peninsula. When the real coastline is included, the formation of anticyclonic eddies along the east side is also observed.

d. Density balance

In Part I it is found that incident CTWs are energetic enough to generate a temporal-mean distribution of kinetic energy along the gulf that is similar in magnitude to that forced by the wind (Martínez and Allen 2002, manuscript submitted *J. Phys. Oceanogr.*). Some of the energy of the incident waves is used to redistribute water

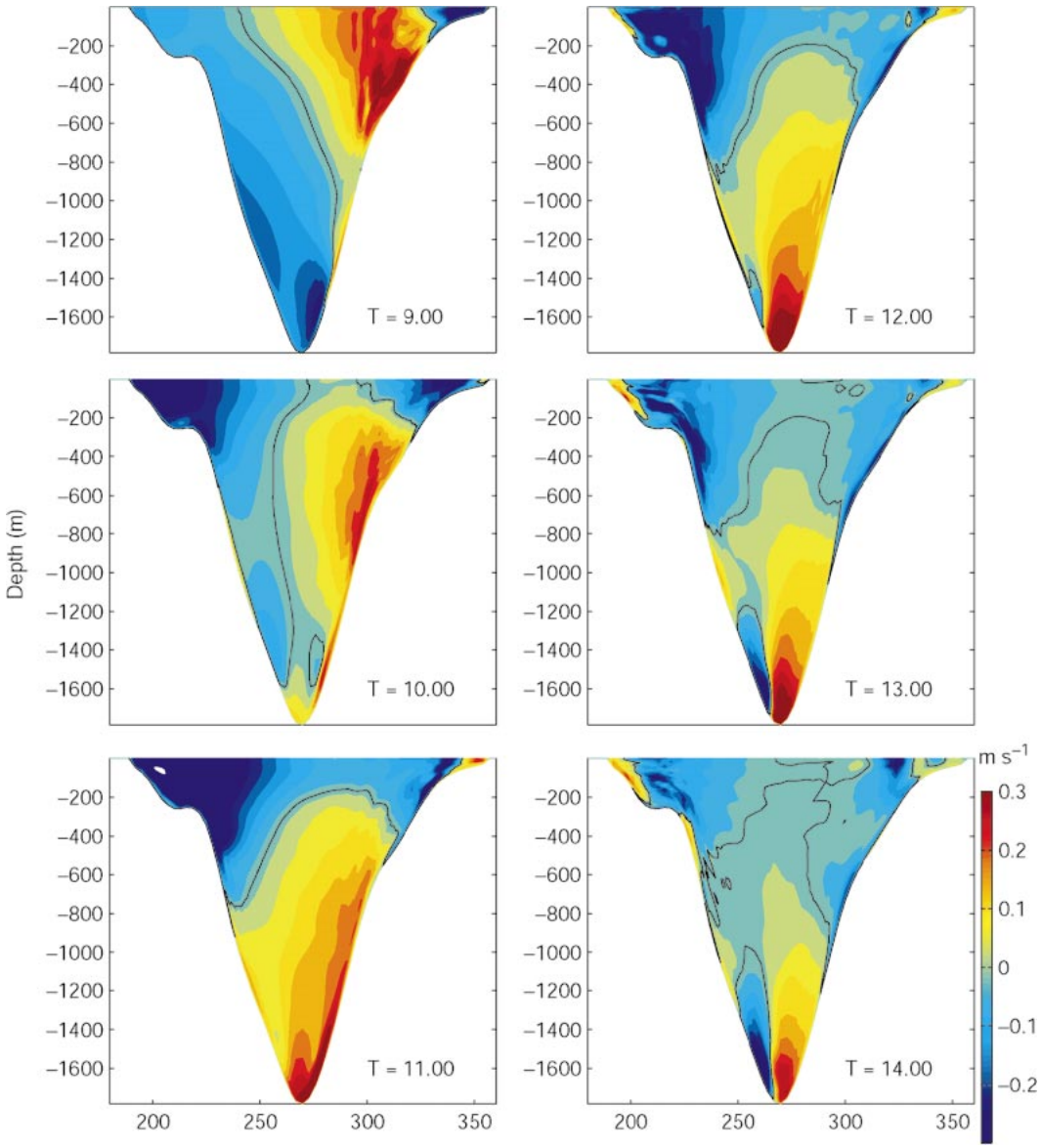

FIG. 15. Across-gulf sections of the along-gulf velocity at $y = 564$ km for days 9–14. The incident elevation wave has an amplitude of 30 cm and a time scale of 4 days as in Figs. 7, 8, and 14. The black line is the zero contour.

masses. Similar to Part I, we examine the resulting density balance by calculating the time-average of the time integral of terms in the density equation, integrated in the across-gulf direction and in depth (e.g., $\Delta y T^{-1} \int_0^T \int_0^t dt' \int \rho_{t'}, dx\, dz$) as a function of y. The results for an experiment with an elevation ICTW of amplitude 16 cm and period 4 days are plotted in Fig. 17. Elevation ICTWs have mean up-gulf northward surface velocities on the east side and weaker down-gulf southward velocities on the west side (Fig. 14), effectively pumping lower-density surface water into the gulf. After the wave exits, the mean density anomaly integrated in (x, z) is negative everywhere except in the northern gulf, producing a net warming along the gulf (Fig. 17). The density flux is positive (down gulf) everywhere, decreasing to the north. The mean density anomaly per volume shows a very uniform distribution north and south of the sill. Near the sill the density anomaly per unit volume has the largest magnitude, indicative of stronger fluxes developed by the changing topography. A depression wave has a similar distribution with the signs reversed and is not shown. The realistic forcing in Part I produces a combination of the results obtained with single elevation or depression ICTWs. The density anomaly is negative south of the sill and positive to the north, changing sign at the sill ($y = 920$ km). This indicates a dominance of the density flux by elevation waves in the south and by depression waves in the north.

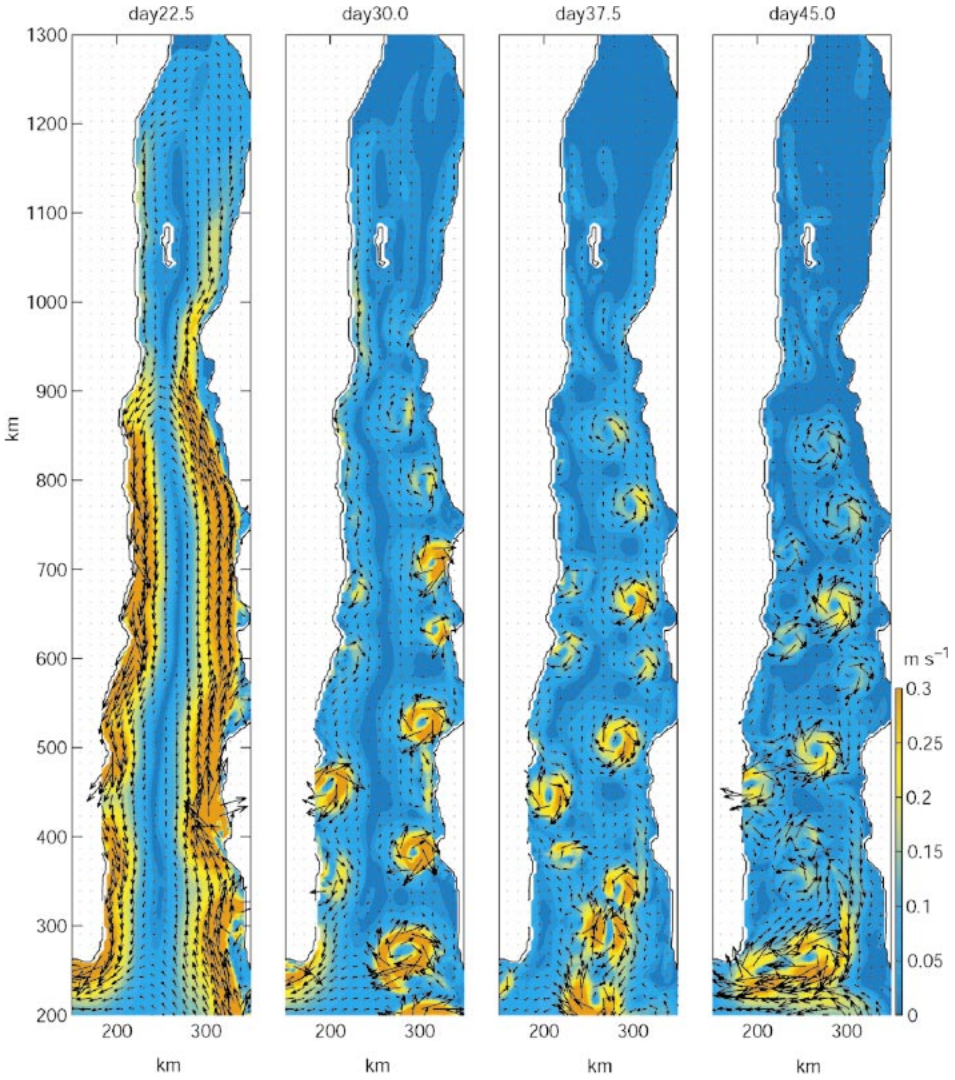

FIG. 16. Surface velocity vectors every 7.5 days from day 22.5 to day 45. The color contours represent the magnitude of the velocity vectors (m s^{-1}). The incident wave has a sea level amplitude of 16 cm and a time scale of 16 days.

5. Summary

A three-dimensional primitive equation circulation model with realistic topography and stratification is used to investigate the propagation of baroclinic coastal-trapped waves (CTWs) in the Gulf of California. The behavior of idealized single incident wave disturbances with different amplitudes and time scales is examined. The numerical results are consistent with the results in Part I and provide new information about the evolution of CTWs in the gulf. As found in Part I, an incident CTW enters the gulf and propagates northward along the east side of the south gulf with no significant changes in propagation characteristics. At the sill the wave splits and most of the wave energy is steered so that it propagates southward down-gulf along the west side. Only a small fraction of the wave energy enters the shallow north gulf where two types of behavior are found: 1) a relatively slow disturbance, with a clear but weak velocity signal that is consistent with a trapped wave, propagates northward along the east coast and eventually dissipates in the far north and 2) a very fast sea level signal propagates and spreads over the entire northern region.

Sea level near the entrance of the gulf (Topolobampo) is well correlated (>0.9) with sea level everywhere inside the gulf (Figs. 1 and 2). Velocity correlations between Topolobampo and locations around the gulf decrease as the wave propagates. The ratio of maximum sea level amplitudes and velocity magnitudes for the waves exiting the gulf in comparison with those for the incident waves is larger for elevation than for depression waves (Fig. 4). Most of the dissipation due to bottom

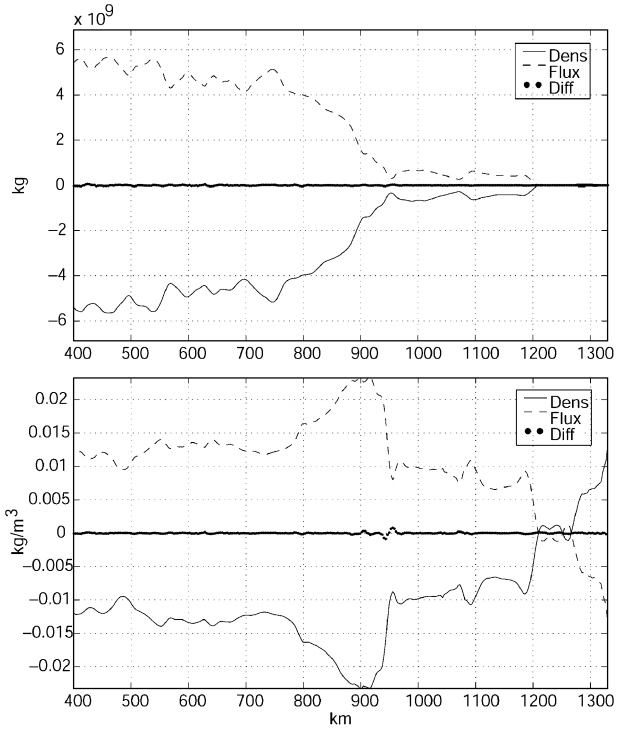

FIG. 17. The along-gulf distribution of the density balance. The terms in the density equation are labeled Dens = time rate of change of density, Flux = advective flux of density, and Diff = diffusion. (top) The time-average of the time integral of the terms in the density equation, integrated in the across-gulf direction and in depth, plotted as a function of *y*. (bottom) The same terms divided by the volume ($\Delta y \int dx\, dz$) of the across-gulf section.

friction takes place at the sill (Fig. 9). No significant bottom dissipation is found in the region north of the sill for any amplitude or time scale of the ICTW.

Incident waves with realistic amplitudes exhibit several nonlinear properties. The propagation velocity increases with amplitude and waves with a large, but realistic, amplitude steepen. A depression wave with large negative amplitude takes almost two more days to propagate from Topolobampo to La Paz than an elevation wave with large positive amplitude (Fig. 3). Steepening of the wave is observed in sea level and in velocity. In general, time series of sea level signals are relatively smooth (Fig. 10) and are not strong indicators of the nonlinear processes that take place. Along-gulf velocity time series are a somewhat better indicator of nonlinear processes; for example, steepening is a little more evident in the alongshore velocity signal (Fig. 11). The strongest indicators of wave steepening are time series of the vertical displacement of isopycnals (Fig. 12). For example, as a large-amplitude elevation wave propagates, the gradients in the isopycnal displacements increase, some higher-frequency fluctuations are generated, and the gradients decrease before increasing again (Fig. 12). This behavior suggests that, as the wave steepens and nonlinear terms become significant, partial breaking takes place and energy is dissipated, smoothing the wave.

Large-amplitude elevation waves on the east side generate a down-gulf countercurrent adjacent to the coast. The countercurrent is strong enough to separate the up-gulf current in the tail of the wave from the coast (Fig. 14). After the wave passes, the circulation consists of a down-gulf current next to the coast and an up-gulf current offshore (Fig. 8). The up-gulf current slowly separates from the coast and propagates offshore and vertically downward along the bottom (Fig. 15). Variable coastline, shelf–slope topography, and nonlinear effects are required for the separation to take place.

Coastal-trapped waves with long time scales, or large-amplitude waves of any time scale, generate eddies along the coast. The eddies have scales of 50–80 km and typically extend vertically to depths of 150–500 m. Elevation waves generate anticyclonic eddies, while depression waves produce cyclonic eddies. Elevation waves produce a larger number of eddies than similar-amplitude depression waves. After the wave passes, the eddies are observed to last at least 25 days. No eddy formation is observed north of the sill (Fig. 16).

Acknowledgments. This research was supported by the Office of Naval Research (ONR) Coastal Dynamics Program through Grants N00014-93-1-1301 and N00014-02-1-0100. In addition, JAM was partially supported by a Fulbright-LASPAU scholarship and by the Facultad de Ciencias Marinas UABC. The use of computational resources (CM500e) provided by the College of Oceanic and Atmospheric Sciences and facilitated by NASA Grant NAG5-11125 (to M. Abbott) and by ONR Grant N00014-99-1-0040 and NSF Grant OCE-952095b (both to A. Bennett) was indispensable for the completion of this research and is gratefully acknowledged. We thank M. Merrifield and C. Winant for providing the velocity and bottom pressure measurements described in Merrifield and Winant (1989) and K. Brink for helpful comments. The authors also thank C. Vandetta and T. Leach for assistance with computer use, P. Newberger for guidance with the POM, and F. Beyer for help with the manuscript preparation.

REFERENCES

Badan-Dangon, A., C. J. Koblinsky, and T. Baumgartner, 1985: Spring and summer in the Gulf of California: Observations of surface thermal patterns. *Oceanol. Acta,* **8,** 13–22.

Blumberg, A. F., and G. L. Mellor, 1987: A description of a three-dimensional coastal ocean circulation model. *Three-Dimensional Coastal Ocean Models,* Vol. 4, N. Heaps, Ed., Amer. Geophys. Union, 1–16.

Brink, K. H., and D. C. Chapman, 1987: Programs for computing properties of coastal-trapped waves and wind-driven motions over the continental shelf and slope. 2d ed. WHOI Tech. Rep. 87-24, Woods Hole Oceanographic Institution, Woods Hole, MA, 119 pp.

Christensen, N., Jr., R. de la Paz, and G. Gutiérrez, 1983: A study of sub-inertial waves off the west coast of Mexico. *Deep-Sea Res.*, **30,** 835–850.

Emilson, I., and M. A. Alatorre, 1997: Evidencias de un remolino ciclónico de mesoescala en la parte sur del Golfo de California. *Contribuciones a la Oceanografía Física en México*, Monografía 3, Unión Geofisica Mexicana, 173–182.

Enfield, D. B., and J. S. Allen, 1983: The generation and propagation of sea level variability along the Pacific coast of Mexico. *J. Phys. Oceanogr.*, **13,** 1012–1033.

Figueroa, J. M., S. G. Marinone, and M. F. Lavin, 2003: A description of geostrophic gyres in the southern Gulf of California. *Nonlinear Processes in Geophysical Fluid Dynamics*, O. U. Velasco Fuentes et al., Eds., Kluwer Academic, 237–255.

Grimshaw, R., 1977: Nonlinear aspects of long shelf waves. *Geophys. Astrophys. Fluid Dyn.*, **8,** 3–16.

Kundu, P. K., 1976: Ekman veering observed near the ocean bottom. *J. Phys. Oceanogr.*, **6,** 238–242.

Martínez, J. A., and J. S. Allen, 2004: A modeling study of coastal-trapped wave propagation in the Gulf of California. Part I: Response to remote forcing. *J. Phys. Oceanogr.*, **34,** 1313–1331.

Merrifield, M. A., 1992: A comparison of long coastal-trapped wave theory with remote-storm-generated wave events in the Gulf of California. *J. Phys. Oceanogr.*, **22,** 5–18.

——, and C. D. Winant, 1989: Shelf circulation in the Gulf of California: A description of the variability. *J. Geophys. Res.*, **94** (C12), 18 133–18 160.

Mitsudera, H., and R. Grimshaw, 1990: Resonant forcing of coastally trapped waves in a continuously stratified ocean. *Pure Appl. Geophys.*, **133,** 635–664.

Pegau, W. S., E. Boss, and A. Martinez, 2002: Ocean color observations of eddies during the summer in the Gulf of California. *Geophys. Res. Lett.*, **29,** 1295, doi:10.1029/2001GL014076.

Ramp, S. R., J. McClean, C. A. Collins, A. J. Semtner, and K. A. S. Hays, 1997: Observations and modeling of the 1991–92 El Niño signal off central California. *J. Geophys. Res.*, **102** (C3), 5553–5582.

Smith, R., 1972: Nonlinear Kelvin and continental shelf waves. *J. Fluid Mech.*, **52,** 379–391.